Dormancy of disseminated prostate cancer cells in the bone cortex is induced by osteoblasts

Ruihua Liu[1,2#], Shang Su[2#], Ke Liu[3,4], Jing Xing[3], Mary Stangis[2], Diego P. Jacho[5], Eda D. Yildirim-Ayan[5], Haiquan Yu[1], Bin Chen[3], Xiaohong Li[2*]

[1]The State Key Laboratory of Reproductive Regulation and Breeding of Grassland Livestock (RRBGL), Inner Mongolia University, Hohhot, 010070, China; [2]Department of Cell and Cancer Biology, College of Medicine and Life Sciences; [3]Department of Pediatrics and Human Development, College of Human Medicine, Michigan State University, Grand Rapids, MI, 49503; [4]Current address: Department of Bio-statistics, School of Public Health, Cheeloo College of Medicine, Shandong University, Jinan, 250001, China,; [5]Bioengineering Department, the University of Toledo, Toledo, OH, 43606

Keywords: prostate cancer, tumor removal, dormancy, bone, osteoblasts, NR2F1, mitochondria

Running title: Osteoblasts induce prostate cancer cell dormancy

Financial support: Shang Su, Mary Stangis, and Xiaohong Li are supported by National Cancer Institute (R01CA230744).

# These authors contributed equally.

*Corresponding author: Xiaohong Li, Department of Cell and Cancer Biology, College of Medicine and Life Sciences, the University of Toledo, 3000 Transverse Drive, Toledo, OH 43614. Phone: +1-419-383-3982; E-mail: xiaohong.li@utoledo.edu

Conflict of Interest Disclosure: The authors declare no potential conflicts of interest.

Abstract

Primary prostate cancer (PCa) cells can disseminate early and stay dormant in distant organs but reactivate later, causing lethal metastasis and recurrence, but the mechanisms of PCa dissemination and dormancy remain elusive. Using C4-2B PCa subcutaneous xenograft mouse model, we observed that the disseminated tumor cells (DTC) were enriched in the bones after tumor removal, more specifically, in the bone cortex. We hypothesized that DTC are dormant in the bone cortex and determined osteoblasts as the inducer for PCa dormancy via an *in vitro* mixed co-culture model. Through RNA-sequencing we defined a unique PCa dormancy gene signature with significantly decreased mitochondrial gene expressions and mitochondria-related functions, which was positively associated with clinical PCa progression. We further predicted dormancy-mimicking drugs using a novel artificial intelligence (AI) platform and validated PF-562271, a focal adhesion kinase (FAK) inhibitor, as dormancy-mimicking *in vitro*. Altogether, our study revealed for the first time the effects of primary tumor removal on PCa cell dissemination, profiled the osteoblasts-induced C4-2B cell dormancy, and induced PCa cell dormancy *in vitro* using AI predicted drugs, which could potentially inhibit PCa bone metastasis progression and recurrence clinically.

Introduction

Prostate cancer (PCa) is the most diagnosed cancer and the second leading cause of cancer death in men in the United States [1]. Up to 90% of advanced-stage PCa patients died with bone metastases, but only 10% of these patients were found with bone metastases at the time of diagnosis [2, 3, 4]. Primary PCa cells can disseminate early and stay dormant/quiescent in distant organs but reactivate later, causing metastasis and recurrence [5, 6, 7, 8]. 20-45% of these patients relapse years later despite various treatments, including prostatectomy and enzalutamide [9, 10, 11, 12, 13]. The mechanisms of PCa cell dissemination, dormancy, and reactivation are overlooked, especially the mechanisms by which various treatments effect on these processes.

Tumor dormancy is categorized into tumor mass dormancy and cellular dormancy [7, 14, 15]. Tumor mass dormancy refers to a state when a small and undetectable tumor reaches an equilibrium of proliferation and cell death, resulting in no progression or overt metastases. Cellular dormancy, or cancer cell dormancy, depicts when a cancer cell enters a state of quiescence with significantly less proliferation. Tumor dormancy is often a mixture of both, and the mechanisms of tumor dormancy can be explained by cancer cell intrinsic quiescence and acquired quiescence resulting from the microenvironment [16, 17, 18, 19, 20, 21, 22, 23]. It is generally accepted that the dormant cells are under cell cycle arrest, neither actively proliferative nor apoptotic, express decreased levels of Ki67 and cell cycle related genes, but express increased levels of dormancy makers such as the orphan nuclear receptor, nuclear receptor subfamily 2 group F member 1 (NR2F1) [23, 24, 25, 26, 27, 28, 29, 30]. Due to cancer cell heterogeneity, it’s reasonable to expect distinct dormancy markers under different microenvironment settings and for various types of cancers.

We aim to uncover the clinically relevant dormant PCa profiles, to answer the questions of whether and how harnessing dormancy inhibits bone metastatic progression and relapse.

In this study, we used C4-2B PCa subcutaneous xenograft mouse model and compared the human disseminated tumor cells (DTC) abundancy in various mouse organs before and after tumor removal. We determined which bone stromal cell keeps PCa cell dormancy using an *in vitro* mixed co-culture model and profiled the dormant C4-2B cells by comparative transcriptomics. We revealed that the top 6 enriched biological processes from the significant down-regulated DE genes were all mitochondria-related. Excitingly, we found increased mitochondria-related biological processes in the up-regulated genes of bone metastases and circulating tumor cells from PCa patients, suggesting a correlation between the dormancy gene signature and better clinical outcome. Therefore, we aimed to identify dormancy-mimicking drugs to induce PCa cells into dormancy. Using a novel drug prediction artificial intelligence (AI) platform, we predicted PF-562271 (PF-271), a potent, ATP-competitive, and reversible focal adhesion kinase (FAK) inhibitor [31, 32, 33] and validated its dormancy-mimicking effect *in vitro*. Altogether, our study revealed for the first time the effects of primary tumor removal on PCa cell dissemination, profiled the gene signature of the osteoblast-induced C4-2B cell dormancy, and identified drugs, which induced PCa cell dormancy *in vitro* and could possibly inhibit PCa bone metastasis progression and recurrence.

Results

DTC were detected early in various organs and tumor removal caused detectable DTC only in the bone cortex

To profile PCa cell dissemination, we injected human PCa C4-2B/Luc cells subcutaneously into immunodeficient NSG mice and monitored tumor growth by bioluminescent imaging and caliper measurement. At 2 weeks post injections, all subcutaneous tumors reached similar sizes in host mice (within the range of 144+/-37 mm^3), then the mice were randomly assigned to three groups (**Figure 1A**). The mice in Group 1 were sacrificed at the 2-week point, Group 2 (termed as Control group) maintained the tumors, and Group 3 (termed as Tumor removal group) underwent tumor removal surgery. Mice in Group 2/3 were monitored weekly till 6 or 8 weeks (to represent late stages of primary tumors) for organ harvest. Luminescent signals of tumor growth increased in mice from the Control group but remained absent in mice from the Tumor removal group (**Figure 1B**). Based on species-specific PCRs (2 µg DNA as input) to semi-quantify the DTC numbers (**Figure 1C**), we found that DTC appeared as early as 2 weeks post injection in various organs examined, such as liver, lung, and bones, etc. (**Figure 1D and Supplementary Figure S1**). The estimated DTC numbers were only 2-10 cells/2 µg DNA for most organs at 2-week (**Supplementary Figure S2**). In mice from the Control group, DTC were consistently detectable in most of the organs examined and an overall increasing trend of DTC could be observed in the organs at week 6 and week 8 compared to week 2, implying that PCa dissemination increases along with primary tumor growth (**Supplementary Figure S2**). In mice of the Tumor removal group, less DTC were detected, compared to those in Control group, supporting that primary tumor removal reduces the overall cancer burdens. However, to our surprise, when the tumors were removed, DTC were only detected in the tibiae and femurs (also skeletal muscles obtained

from the hind limbs in certain mouse) at week 6, suggesting a possible enrichment or preference of DTC at the long bone sites. At week 8, DTC were further detected in the prostate, skull, but were still estimated to be most abundant in tibiae (i.e., average of 100 cells/2 μg DNA) among these organs with DTC (**Figure 1D and Supplementary Figure S2**). No significant changes of DTC in tibia/femur/skeletal muscles of week 8 compared to the ones of week 6 in the Tumor removal group were observed, but the DTC numbers were significantly increased at week 6 or week 8 when compared to those at week 2 (**Supplementary Figure S2)**. These data revealed that PCa cells could disseminate to various organs early when the tumors were only ~100 mm^3 and the overall DTC were increased time-dependently. After tumor removal, the overall amounts of DTC dropped, and DTC were obviously enriched in bones and bone-associated skeletal muscles at the time points examined.

Focusing on the long bones, we separated the bone marrow from the bone cortex of the tibiae via centrifugation (**Figure 2A**). DTC were detected in the bone cortex, but not in the bone marrow at week 2 and week 6 from mice of both groups (i.e., Group 2 &3), and appeared at week 8 in the bone marrow from mice in the control group (**Figure 2B**). However, in mice from tumor removal group, DTC were still only detectable in the bone cortex at week 8 (**Figure 2B**). Note that the DTC in the bone marrows were also confirmed at cellular level using IF (immunofluorescence) staining the whole human mitochondria (**Figure 2C**), indicating the presence of viable and intact DTC. These data revealed that DTC arrived in the bone cortex prior to the bone marrow, or better survived in the bone cortex. Tumor removal limited and enriched DTC in bones, exclusively in the bone cortex, at least at the times examined. Since DTC and

tumor mass were found in the bone marrow in both patients and animal models with overt bone metastasis, we hypothesize that DTC are dormant in the bone cortex.

Osteoblasts, but not other stromal/bone cells, inhibited PCa cell proliferation

To test our hypothesis that DTC are dormant in the bone cortex, we mixed and co-cultured PCa C4-2B/GFP cells (written as C4-2B in the following co-culture context if not specified) with various stromal cells to model and delineate stromal/bone cell effects on DTC. C4-2B cell proliferation was monitored by the GFP signals via IncuCyte imaging (**Figure 3A**). In comparison with C4-2B cultured alone, we found that only MC3T3-E1 (MC3T3) murine osteoblasts inhibited C4-2B cell proliferation in the co-culture (**Figure 3B**). NIH3T3 fibroblasts, RAW264.7 macrophages, or OP-9 mesenchymal stem cells showed no significant effect on C4-2B cell proliferation. HUVEC endothelial cells and MLO-Y4 osteocytes, on the other hand, promoted C4-2B cell proliferation. Using membrane dye labelling and flow cytometry (FACS), we found that C4-2B cells with high dye intensity (indicating less cell divisions) accounted for at least 90% of total C4-2B cells in the mixed co-culture vs 20% in C4-2B cultured alone (**Figure 3E**). Similarly, the proliferation of PC-3 was also inhibited by MC3T3-E1 cells, measured by Incucyte and FACS using membrane dye labelling (**Supplementary Figure S3A&B**). To get more details about the cell cycle distribution in the co-cultured cells, we labelled C4-2B cells with PIP-FUCCI (Fluorescent Ubiquitination-based Cell Cycle Indicator), a dual fluorescence indicator designed for cell cycle phase labelling [34]. Pure green and red fluorescence signals in PIP-FUCCI-labelled cells indicate cells in G0/G1 and G2/M phases, respectively. We found that in the mixed co-culture, 70% of the total C4-2B cells were in G0/G1 and 25% were in G2/M, while in the C4-2B cultured alone, 25% of the total C4-2B cells were in G0/G1 and 40% in

G2/M (**Figure 3C**). These data suggest that MC3T3-E1 cells inhibited C4-2B cell division through inducing G0/G1 arrest. To rule out the effect of apoptosis for less C4-2B cell proliferation, we found that 5% of the total C4-2B cells were apoptotic in the mixed co-culture and 18% of the total C4-2B cells were apoptotic in C4-2B cultured alone, suggesting that MC3T3-E1 cells did not induce, instead inhibited, C4-2B cell apoptosis (**Figure 3D**). H_2O_2 treatment for 2 hours (serving as a positive control) induced 50% of the total C4-2B cells apoptosis.

To determine whether physical contacts between PCa cells and osteoblasts are necessary and whether secreted factor(s) could play a role for the proliferation inhibition, we collected conditioned media (CM) from the mixed co-cultures, CM from either C4-2B cells or MC3T3-E1 cells cultured alone, and CM from transwell co-culture, and applied these CM to C4-2B cells. We found that only CM from the mixed co-culture significantly inhibited C4-2B proliferation (**Figure 3F**), suggesting that the physical contacts among C4-2B cells and MC3T3-E1 cells are required. Together, these data suggest that when in the physical contact with PCa cells, osteoblasts, but not other stromal/bone cells tested, inhibit PCa cell proliferation through cell cycle arrest, but not inducing the apoptosis. This effect could be mediated, at least in part, by secreted factor(s) activated upon mixed co-culture.

Osteoblasts increased the expression of dormancy marker and decreased the expression of proliferation markers

We found that one of the dormancy markers, *NR2F1* (*Nuclear Receptor Subfamily 2 Group F Member 1*) [30], was significantly increased at mRNA level in the mixed co-cultured C4-2B cells,

compared to C4-2B cultured alone. In contrast, the proliferation markers, Ki67 and cyclin D1, were both decreased (**Figure 4A**). The increase of NR2F1 was also confirmed at the protein level (**Figure 4C, right panel**). Note that the current available antibodies for NR2F1 are not species-specific, so we separated the C4-2B cells from the mixed co-culture for the western blotting. The separation of cells was validated and confirmed by fluorescence microscopy (for C4-2B/GFP) (**Figure 4B**) and species-specific PCR (**Figure 4C, left panel**).

To closely recapitulate the *in vivo* microenvironment, we advanced our 2D mixed co-culture to 3D, in which the C4-2B and MC3T3-E1 cells were embedded in type I collagen and mixed co-cultured, because the type I collagen forms 90% of the organic mass of bone [35, 36]. Increased NR2F1 expression and decreased Ki67 and cyclin D1 expressions were observed in this 3D mixed co-culture compared to C4-2B cultured alone at the same 3D condition (**Figure 4D**), suggesting consistency between the 2D and 3D mixed co-cultures in modeling interactions between osteoblasts and C4-2B cells. For convenience, we continued using the 2D mixed co-culture in our studies.

We further explored whether and how cell number ratio and co-culture time in the mixed co-cultured of C4-2B and MC3T3-E1 cells affect the dormancy induction efficiency in this model. We observed the concurrent increase of NR2F1 and decreases of Ki67 and Cyclin D1 at various C4-2B:MC3T3-E1 ratios (ranging from 1:30 to 1:6) (**Figure 5A**). Decreases of Ki67 and increase of NR2F1 were also detected in day 3 to day 6 (or 72 to 144 hours since mixed co-culture) co-cultures (**Figure 5B**). NR2F1 increases at protein level were further confirmed from day 3 to day 6 at the ratio of 1:30 of the C4-2B:MC3T3-E1 cells (**Figure 5C**).

Osteoblasts decreased mitochondria-related genes in the mixed co-cultured C4-2B cells

To profile the dormancy-like C4-2B cells in the mixed co-culture, we performed RNA-sequencing to determine the DE genes in relative to C4-2B cultured alone. Since the mixed co-culture samples generated transcripts in both human and mouse species, we applied three independent bioinformatic pipelines, Xenome [37], Xenofilter [38], and Kallisto [39], to enrich human-specific reads out of the raw sequencing data and then applied DESeq2 to identify the common (overlapped) DE genes, from which the biological process enrichment using Gene Ontology (GO) was annotated (**Figure 6A**). The top 6 enriched biological processes from the significant down-regulated DE genes were all mitochondria related, such as oxidative phosphorylation, energy coupled proton transmembrane transport, mitochondrial ATP (adenosine triphosphate) synthesis coupled electron transport, etc. (**Figure 6B**). Notably, all of the 13 mitochondria-encoded protein-coding genes were down-regulated at mRNA level in the mixed co-cultured C4-2B cells in RNA-Sequencing results and we confirmed the decreases of the representative genes, i.e., *MT-ATP6 (ATP synthase membrane subunit 6)*, *MT-ND1,2&4 (NADH:Ubiquinone oxidoreductase core subunit)*, *MT-CYB (cytochrome B)*, and *MT-CO1 (cytochrome C oxidase I)*, using qRT-PCR with human-specific primers (**Figure 6C**). We also isolated the total genomic DNA of C4-2B cells cultured alone and co-cultured and performed qPCR to calculate the mitochondrial DNA (mtDNA) copy [40]. We found that the mtDNA copy number was downregulated in the mixed co-cultured C4-2B cells (**Figure 6D**). These data suggest that the down-regulated mitochondrial genes may be a result of an overall decrease of mitochondrial DNA copy number due to the induction of osteoblasts. These data also suggest the down-

regulated mitochondrial genes and enrichment of mitochondria-related biological processes as novel dormant cell markers.

To explore the potential clinical relevance of our novel PCa dormancy findings, we analyzed the published patient datasets. Excitingly, we found that the upregulated DE genes in circulating PCa tumor cells, in comparison to the primary tumors, are enriched to the mitochondrial structural components (data processed from previously published study [41], **Figure 7A**). High *MT-ND1* gene expression has a favorable prognostic trend in PCa patients with bone metastases (**Figure 7B**, from cBioportal study ID: prad_su2c_2019). These clinically relevant data suggest a reverse correlation between mitochondrial genes and enrichment of mitochondria-related biological processes, and PCa progression.

Mitochondrial inhibitors inhibited C4-2B cell proliferation, but did not induce cell dormancy

To determine whether mitochondrial inhibition could induce the same dormancy-like phenotypes of C4-2B as osteoblasts in the mixed co-culture did, we chose to test some well-established mitochondrial inhibitors. We found that rotenone or IACS-010759 (both are respiration complex I inhibitors), and FCCP, a potent uncoupler of oxidative phosphorylation in mitochondria, inhibited C4-2B proliferation in a dose-dependent manner (**Supplementary Figure S4A**). However, rotenone or IACS-010759 significantly decreased the expression of dormancy marker NR2F1 at 24 to 72 hours (**Supplementary Figure S4B)**. At 72 hours, FCCP also decreased the expression of NR2F1 but increased the expressions of *Ki67*, *Cyclin D1*, *MT-ND1*, and *MT-CO1*

(**Supplementary Figure S4C**), suggesting that mitochondrial inhibition could not induce PCa cell dormancy.

Taken together, these data profiled that the dormant-like C4-2B cells induced by physical contact with osteoblasts displayed known dormancy features including NR2F1 increase and Ki67/Cyclin D1 decreases, and interesting novel features as mitochondria-related gene suppressions. However, mitochondrial inhibitors could not recapitulate the dormancy-like phenotype, i.e., the expressions of dormancy markers, suggesting the enrichment of the decreased mitochondria-related biological processes is likely a result, but not a cause of osteoblasts-induced PCa cell dormancy.

AI predicted dormancy-mimicking drug, PF-562271, but not PIK-75, induced C4-2B cell dormancy

We used a newly-developed AI (artificial intelligence) platform (developed and unpublished by Dr. Bin Chen and collaborators) to predict drugs that mimic our dormant DE gene signature. Briefly, the dormant PCa DE genes were compared against a database of drug-induced gene expression matrix, and the drugs were scored according to the similarities between drug-induced gene expression profiles and the dormant PCa gene signature. PF-562271 (also known as PF-271) and PIK-75 were identified as the top dormancy-mimicking drugs (**Figure 8A**). PF-271 is a reversible, ATP-competitive focal adhesion kinase inhibitor [31, 32, 33]. We found that PF-271 inhibited C4-2B proliferation dose-dependently (**Figure 8B**), induced G0/G1 phase arrest by FUCCI analysis (**Figure 8C**), induced the expression of NR2F1 (at mRNA and protein level), decreased the expressions of Ki67 and Cyclin D1 at mRNA levels (**Figure 8D&E**), and had no

effect on apoptosis (**Figure 8F**). Together these data suggest that PF-271 induces C4-2B cell dormancy.

Another predicted dormancy-mimicking drug, PIK-75, a PI3K inhibitor [42], also inhibited C4-2B cell proliferation dose-dependently (**Supplementary Figure S5A**). However, PIK-75 induced apoptosis (**Supplementary Figure S5E**) and had no effect on cell cycle arrest (**Supplementary Figure S5B**) or NR2F1 protein expression at 48 and 72 hours (**Supplementary Figure S5C**). PIK-75 did induce the expression of NR2F1 at 48 and 72 hours at mRNA levels, but it also elevated the expressions of proliferation markers, Ki67 and Cyclin D1 (**Supplementary Figure S5D**), confirming that PIK-75 does not have a dormancy-mimicking effect.

Discussion

Opportunities and challenges coexist in obtaining the basic knowledge of cancer dormancy and translating it into patient care [43, 44]. In this study, we revealed the effects of primary tumor removal on PCa cell dissemination and dormancy, and a novel PCa dormancy gene signature, which was reversely correlated with PCa metastatic progression in patients. Importantly, we identified and tested drugs mimicking cancer dormancy that could potentially inhibit and prevent PCa metastatic recurrence.

To our knowledge, this is the first longitudinal examination of organ-specific PCa cell dissemination. DTC were detected in various organs, such as bone, liver, lung, and kidney, which are consistent with the clinically observed PCa metastases [2]. Interestingly, DTC were detected in the bone cortex prior to the bone marrow, surgical removal of the xenografted tumors

limited PCa DTCs only in the bone cortex, at the times examined. Clinically, metastatic PCa tumors were found in the marrows of bone metastatic patients and presence of DTC in the marrow was associated with poor prognosis [45]. These data suggest that DTC might be dormant in the bone cortex. Since we haven't performed IHC to confirm the DTC in bone cortex, it's possible that the detected DTC are circulating tumor cells (CTC). Thorough blood perfusion prior organ harvesting is warranted to rule out this possibility. However, the DTC in mice of tumor removal group clearly showed a preference of DTC in the bone over liver, one of the blood-rich organs, suggesting the detected DTC in mice without perfusion are unlikely CTC and the bone preference of dissemination is consistent with the frequently observed bone tropism of PCa [46]. No significant difference of DTC was found between mice with and without xenografted tumor removal, suggesting PCa cells disseminate earlier, i.e., prior to tumor removal, and DTC do not quickly proliferate nor die. However, it's possible that this could be due to limited animal numbers in each group. The semi-quantitative PCR method we have optimized provides a cost-effective approach and accessible platform to evaluate the trends of PCa cell dissemination. It will be interesting to apply this method in further investigating how other therapies, such as chemotherapy, first-line ADT drugs, or androgen receptor antagonist enzalutamide, affect PCa cell dissemination and dormancy.

Using both 2D and 3D *in vitro* co-culture of PCa and various types of cells of the bone microenvironment, we found that osteoblasts' direct physical contact with PCa cells are necessary and sufficient to induce PCa cells into dormancy-like status. This is consistent with previous report using different approaches [47, 48]. The direct co-culture of PCa cells and

osteoblasts provided an easy platform for rapid screening of drug candidates that can modulate PCa dormancy. We recognized the limitation that it oversimplified in terms of the complicated bone microenvironment. Co-culture of PCa cells with more types of cells from the bone microenvironment in a bone graft or scaffold with mechanical loading is better models to explore in the future. The conditioned media (CM) from directly mixed co-culture induced partial growth inhibition of C4-2B cells but CM from non-contact transwell co-culture did not affect C4-2B growth at all, suggesting that both secreted factors stimulated by physical contact co-culture and signaling at the C4-2B/MC3T3 interface were responsible for dormancy induction. In fact, we noticed the functional enrichment of KEGG pathway "Cell adhesion molecules" in up-regulated DE in dormant cells (**Supplementary Table S5**). Moreover, the dormancy-mimicking drug PF-271 *per se* is an inhibitor of focal adhesion kinase and inhibition of FAK was reported to be sufficient to prevent tight junction disruption [49], implying that cell-cell interaction such as adhesion and tight junction might play a vital role in establishing PCa dormancy. How osteoblast-PCa interaction results in PCa dormancy will be further investigated.

Dormant cancer cells' signatures have been reported in several studies, which provided important knowledge in the field [23, 50, 51, 52, 53]. However, the limitations include that none of them was characterized in the context of the bone microenvironment, and the signatures are limited in patient number and patients from one center. More studies are needed to reveal and validate the signatures for PCa, especially in the context of the bone microenvironment. Our study contributed to PCa dormant signature in the context with osteoblasts. Consistently, NR2F1 was shown as a marker for dormant cancer cells [30, 54, 55, 56, 57]. In our dormant C4-2B DE genes, we found that some stem cell markers, including ALDH1A1 and BCL11B, were significantly. Other

stem cell markers, such as BMI1 and SOX2 [58, 59], were not changed. Dormant head and neck squamous cancer cell marker, SOX9 [30], was significantly decreased (**Supplementary Figure S6 & Table S3**). Together, these data showed that the dormant cancer cells share some gene expression but are distinct, possibly due to the intrinsic features and/or in response to different tumor microenvironment. Importantly, the bone niche, specifically osteoblasts, might render the dormant PCa cells a unique gene signature, which might be specific to bone metastatic progression and relapse. For example, the mitochondrial functional term enrichment was identified in the down-regulated DE of the dormant C4-2B gene signature, while mitochondrial functional term enrichment in up-regulated DE were found in PCa metastases and CTC, respectively, in recent publication [60] and by our own dataset analyses. These data suggested the functional role of the dormant C4-2B signature in bone metastatic progression and relapse. Therefore, this signature can be used to discover drugs that could mimic or reverse PCa cell dormancy, for the understanding of basic biology and potential treatment and prevention of bone metastasis and relapse. Considering that the dormant PCa cells cause no symptoms in patients, it has been a proposed idea that maintaining cancer cell dormancy can be an operational cure for cancer patients.

Based on the decreases of all mitochondria-encoded genes in dormant C4-2B cells, we speculated that either the mitochondrial overall transcription was inhibited and/or the gene copy number was reduced. Indeed, we found that the mitochondrial gene copy number was reduced in the co-cultured dormant C4-2B cells, but not the expression of factors directly responsible for mitochondrial gene transcription, such as TFAM, TFB1M, or POLRMT. Furthermore, although mitochondrial gene signature was validated functionally in patient data, direct mitochondria

inhibition was not suggested to be a cause of C4-2B dormancy, instead a result of the quiescent PCa cell. We therefore used a novel AI tool (unpublished) to predict dormancy-mimicking drugs. Our initial *in vitro* testing suggested the dormancy-mimicking effect of PF-271. Future studies on the mechanism of action and *in vivo* preclinical testing are needed to determine the translational potential of the drug.

Altogether, our studies revealed the primary tumor removal effect on PCa cell dissemination and dormancy. We identified a functional validated dormant PCa signature, specifically in the context of bone and revealed that the down-regulated mitochondrial genes were new markers for dormant PCa cells. This newly established dormant signature can be used for AI drug screening purpose in identifying drugs or new functions of drugs effects on dormancy-mimicking and dormancy-reversing.

Methods

Cell cultures

Cell lines were purchased from ATCC (American Type Culture Collection, Manassas, VA) unless specified. Mouse osteoblast MC3T3-E1 cells (gift from Dr. Bart Williams, Van Andel Institute) were maintained in α-MEM supplemented with 10% fetal bovine serum (FBS). Mouse macrophage Raw264.7 cells (gift from Dr. Cindy Miranti, Arizona State University), mouse fibroblast NIH3T3 cells, and human embryonic kidney 293FT cells were maintained in DMEM/HG supplemented with 10% FBS. Mouse mesenchymal progenitor OP-9 cells (gift from Dr. Tim Triche, Van Andel Institute) were cultured in MEM-α supplemented with 20% FBS. Murine Osteocyte-like Cell Line MLO-Y4 were grown in α-MEM supplemented with 5% FBS and 5% calf serum (CS) on the plate pre-coated with rat tail type 1 collagen (0.15 mg/mL, Corning, Corning, NY). Human PCa cell lines, C4-2B (gift from Dr. Leland Chung and purchased from ATCC) and PC-3, were cultured in RPMI-1640 supplemented with 10% FBS. Human primary umbilical vein endothelial cells (HUVEC) were cultured in vascular cell basal media supplemented with BBE endothelial cell growth kit components. All the cells were authenticated using STR profiling in LabCorps (Burlington, NC) and maintained mycoplasma-free. Stable cell lines were generated via lentivirus infection as described in the sections below.

Lentivirus packaging and stable cell line generation

pLenti-GFP-Blast (gift from Dr. Wei Wu, Tsinghua University) was used for general GFP labelling and pLenti-PGK-Neo-PIP-FUCCI (Fluorescent Ubiquitination-based Cell Cycle Indicator) (Addgene) was used for accurate cell cycle phase indicator [34]. Luciferase-expressing lentiviral particles (puromycin resistance) were purchased from GeneCopoeia (Rockville, MD).

All the other lentiviral supernatants for stable line generation were prepared in 293FT cells using ViraPower™ Lentiviral Gateway™ Expression Kit (Thermo Fisher) following the manual. C4-2B were infected with virus particles/supernatants, selected with blasticidin, puromycin, or neomycin for 7-10 days to get stable cell populations, and later maintained at low antibiotic concentrations. C4-2B/Luc cells were treated with D-Luciferin (GoldBio, St Louis, MO) for 10 min before scanning in the IVIS® Spectrum *In Vivo* Imaging System (PerkinElmer, Waltham, MS) to confirm the luciferase expression. C4-2B/GFP and C4-2B/PIP-FUCCI cells were confirmed via fluorescence microscopy.

Mouse models

NSG-SCID mice were originally purchased from Jackson Laboratory (Bar Harbor, Maine) and then bred and maintained in our animal facility. The research protocols were approved by the Institutional Animal Care and Use Committee (IACUC) under protocol numbers 400066/400131 at the University of Toledo. Male mice 6- to 8-wks old were used for xenografting of human PCa cells. For subcutaneous xenograft models, 1 million C4-2B/Luc cells were suspended in 50 μL PBS, mixed with 50 μL Matrigel, and subcutaneously injected into the left flank of NSG-SCID mice. Luminescent imaging (IVIS, Perkin Elmer, Waltham, Massachusetts) was performed blinded once per week monitoring the tumor growth.

After 2-wks (weeks) post tumor xenografting, the xenografted mice got similar sizes of tumor sizes and were randomized into three groups for DTC detection at different time points. Group 1, the mice were euthanized for organ harvest and DTC detection at 2-wks. Group 2 served as control. Group 3, the mice received surgical removal of the tumors at 2-wks. The mice in Group 2/3 were

monitored, imaged, and euthanized at different time points, i.e., 6- or 8-wks post PCa injections. Various organs/tissues were harvested at end points for genomic DNA extraction and species-specific PCR to detect the disseminated human PCa cells.

For determination of DTC distribution in long bones such as tibiae and femurs, we first removed the skeletal muscles, then cut the bones open at one end and set it into a 0.5 mL open-bottomed centrifuge tube, which was placed inside a 1.5 mL centrifuge tube. The bone marrows were spin out at the maximum speed of a tabletop Eppendorf centrifuge and collected in the 1.5 mL centrifuge tube for further uses, either DNA extraction or immunofluorescence (IF) staining.

Disseminated tumor cells (DTCs) detection

Total DNA was extracted from various mouse organs using NucleoSpin Tissue kit (Macherey-Nagel lnc., Allentown, PA). The DNAs were used for species-specific PCR with primers against human α-satellite and mouse plakoglobin genomic regions [61]. To semi-quantify the DTCs, A standard curve was first established by performing species-specific PCR from total DNA extracted from the mixtures of C4-2B, at 0, 1, 10, 100, 1,000, 10 k, or 100 k of cells, and 3 million MC3T3-E1 cells. 2 µg DNA for human α-satellite or 500 ng DNA for mouse plakoglobin were added as templates respectively. Primers are listed in **Supplementary Table S1**. DNA gel images for verification of species specificity of primers were provided in **Supplementary Data**. The final PCR products were loaded on 2% agarose gel and the band intensities were quantified using Image J (FIJI 1.53c). Human cell numbers were therefore relatively quantified via linear regression based on the intensity ratios of human α-satellite to mouse plakoglobin. This standard is used to semi-

quantify the human cell DTC from the harvested mouse tissues. All DTC quantifications were performed in a blinded manner.

To validate that the DTC in the bone marrow are viable cells, we resuspended the bone marrow cells in the 1.5 mL centrifuge tube, lysed red blood cells with ACK Lysing Buffer (ThermoFisher) and further mounted them onto the slides using Cytospin. Cells on the slides were fixed with 4% Paraformaldehyde (PFA), permeated with 0.2% Triton, and blocked by 3% BSA. Slides were further incubated overnight at 4˚C with primary antibody against human mitochondrial marker. On the second day, the slides were washed three times and further incubated with Alexa Fluor 568 conjugated goat-anti-mouse IgG secondary antibody. Then the cells were stained with DAPI solution and washed three times before mounting with Fluoromount-G® Anti-Fade Mounting Medium (Southern Biotech, Birmingham, AL). Images were captured using Zeiss Observer Z1 confocal microscope (Carl Zeiss, Oberkochen, Germany) and processed using Image J.

***In vitro* co-culture models**

For the mixed co-cultures, stromal cells, MC3T3-E1 ($3x10^5$/well), RAW264.7 ($1x10^5$/well), NIH3T3 ($5x10^4$/well), OP-9 cells ($3x10^5$/well), MLO-Y4 ($3x10^5$/well), or HUVEC ($3x10^5$/well) were seeded in 6-well plate and allowed for adherence for 20 to 24 hours. C4-2B/GFP cells ($1x10^4$/well) were then added. The culture media for corresponding stromal cells were used for co-culture unless specified. Cells were harvested at certain times for further analyses.

For conditioned media (CM) treatment, we collected CM at day 3 from C4-2B, MC3T3-E1, the mixed co-culture of C4-2B and MC3T3-E1 cells, or the transwell co-cultures (MC3T3-E1 cells in

the well and C4-2B cells in the inserts with 0.4 μM pore membrane). For treatment, CM was mixed with fresh α-MEM media at a 1:1 ratio and applied to C4-2B. Cell proliferation was then monitored using Incucyte S3 based on the GFP signals for 3 days.

The 3D co-culture protocol was modified based on previous studies [62, 63, 64, 65]. Briefly, C4-2B cells or the mixture of MC3T3-E1 and C4-2B (30:1) were encapsulated at 10^6 cells/mL seeding density within collagen type I solution (Corning, USA) and neutralized to pH 7~8 with chilled 1N NaOH to a final collagen concentration of 3 mg/mL. The cell-collagen solutions were added to the silicon chambers and polymerized at 37°C for 1 hour, proceeded with adding 1 mL complete media and incubated for 3 days at 37°C and 5% CO2 before harvest for gene expression analyses.

Cell division and cell cycle analyses

To monitor cell divisions, the C4-2B or PC-3 cells were labeled with CellTrace™ Violet (CTV) Cell Proliferation Kit (Thermo Fisher) according to the manufacture's manual. These chemical dyes can be saturated in cells and is diluted into half every time the cell divides. Therefore, intensity of the dye in the cells is an indication of the cell division [51]. The cells with various dye intensities were examined using flow cytometry on a FACS Cytek Aurora flow cytometer and data were analyzed with FlowJo software. DAPI staining was also applied to exclude dead cells. Gating strategies were showcased in **Supplementary Data**. Briefly, cells without DAPI staining were considered as live cells, then cells positively stained with CTV signals were gated as PCa cells. CTV-labeled PCa cells were further gated into Bright and Dim populations according to their signal intensities.

C4-2B/PIP-FUCCI cells were used to monitor the cell cycle [34]. Cells with pure green and pure red fluorescence indicate cells in the G0/G1 and G2/M phases, respectively. We counted the total cells and cells with either green or red color under 20x magnitude at 6 random areas per group. Cell counting was performed in a blinded manner.

Cell Apoptosis Assay

For cell apoptosis, cells were stained with Hoechst 33342 (5 μg/mL, ThermoFisher) at 37°C for 30 min, refreshed with fresh media and captured under fluorescence microscopy. The cell nuclear morphologies from multiple views were recorded and apoptotic nuclei were counted in a blinded manner. C4-2B cells treated with 1 mM H_2O_2 for 2 hours were used as the positive control for apoptosis [66].

RNA extraction and qRT-RCR

Total RNAs from cell culture were isolated with TRIzol (Thermo Fisher) and reversely transcribed into cDNA using the High-Capacity cDNA Reverse Transcription Kit (Thermo Fisher) following the manufacturers' protocols. The quantitative real-time PCR (qRT-PCR) was performed using SYBR Select Master Mix (Bio-Rad). Relative quantities of target mRNA expressions were performed on cycle threshold (*Ct*) values of target mRNAs and the reference gene *GAPDH*, using the $2^{-\Delta\Delta Ct}$ method. Primers are validated and listed in **Supplementary Table S1.**

Mitochondrial gene copy analysis

After 3 days' C4-2B cells cultured alone or C4-2B/MC3T3-E1 mixed co-cultures, DNA were extracted from cells using NucleoSpin Tissue kit (Macherey-Nagel lnc.). Primers against nuclear genome and mitochondrial genome were used for qRT-PCR (sequences provided in **Supplementary Table S1**) and the *Ct* values were used for calculating the mitochondrial gene copies per cell [40].

RNA-Sequencing

Total RNAs were extracted from cells cultured alone or the mixed co-culture using RNeasy kit and were decontaminated of the DNA using RNase-Free DNase Set (Qiagen, Hilden, Germany). Libraries were prepared by the Van Andel Institute Genomics Core from 500 ng of total RNA using the KAPA stranded mRNA kit (v4.16) (Kapa Biosystems, Wilmington, MA). RNA was sheared to 300-400 bp. Prior to PCR amplification, cDNA fragments were ligated to IDT for Illumina UDI adapters (IDT, Coralville, IA). Quality and quantity of the libraries were assessed using a combination of Agilent DNA High Sensitivity chip (Agilent Technologies, Santa Clara, CA) and QuantiFluor® dsDNA System (Promega). Individually indexed libraries were pooled and 50 bp, paired end sequencing was performed on an Illumina NovaSeq 6000 sequencer using 100 cycle sequencing kit (Illumina Inc., San Diego, CA) to a minimum read depth of 40 M reads/library. Base calling was done by Illumina RTA3 and output of NCS was demultiplexed and converted to FastQ format with Illumina Bcl2fastq v1.9.0. The Raw read files can be accessed via GEO (GSE210751).

RNA-Seq data processing

We developed three pipelines, Xenome [37], XenofilteR [38], and Kallisto [39], to process the human-specific gene expression changes from the RNA-Seq data (FastQ) from the mixed co-culture samples. For Xenome, the raw reads were first filtered to keep the human-only reads and then aligned to human reference genome (GRCh38 for human) via HISAT2 [67]and read counts were called using FeatureCounts in the subread package [68]. For XenofilteR, the FastQ files were first split into files of 50 million sequences via the split2 function from the SeqKit toolkit [69], then aligned via HISAT2 to human (GRCh38) and mouse (GRCm38) reference genomes respectively. The sorted bam files for both human and mouse alignment were loaded into XenofilteR to filter out mouse reads and merged for read counts calling via FeatureCounts. For Kallisto, we merged human and mouse transcriptome reference sequences (downloaded from Gencode) and created a cross-species transcriptome index for human-specific gene expression quantification. Raw reads from C4-2B cells cultured alone were also applied into the three algorithms to maintain the same filtering standard for comparative DE analyses. DESeq2 was used in all the three pipelines to perform DE analyses (a gene with |log2FC| >=1 & padj < 0.05 was considered as a DE gene) based on the FeatureCounts files (Xenome and XenofilteR) or gene counts (Kallisto). Genes identified to be DE by at least two pipelines were considered for Gene Ontology (GO) and KEGG enrichment analyses in a blinded manner via EnrichR [70] or ShinyGO v0.61 [71]. The DE lists from all the three pipelines were provided in **Supplementary Table S3**. Codes are available upon request.

Western blotting

Western blotting experiments were performed as previously described [72]. Antibodies were purchased from various companies. The application, the concentration, and the sources of the antibodies were listed in **Supplementary Table S2**. An antibody was selected based on its

validations, including positive and negative controls, and references. Original blot images were provided in **Supplementary Data**.

Reagents, Chemicals, Kits, and plasmids

Listed in **Supplementary Table S4**.

Statistical analysis

Normality of data was determined before performing statistical analyses. For experiments without repeated measures, data were analyzed via two-way ANOVA when there were two independent variables. Otherwise, a two-tailed Student's t-test was used. Analysis and statistical significance of all data sets were determined using GraphPad Prism 9. If not mentioned, two-tailed p value was computed and $p < 0.05$ was considered significant.

Data availability

Raw RNA-Seq read files (FastQ) for C4-2B cultured alone and C4-2B/MC3T3-E1 mixed co-culture are deposited into GEO under accession GSE210751. The sources for the public or published RNA-Seq files processed in this manuscript are mentioned in the context.

Ethics declarations

All the authors declare that they have no conflicts of interest.

Acknowledgments

This work was supported by NCI grant R01CA230744.

Author contributions

XL conceived and directed the project. XL, RL, and SS wrote the manuscript. XL, RL, and SS designed, and performed the experiments. KL, JX, and SS performed the bioinformatic analyses under the support and guidance from BC. RL and SS performed the statistical analyses. DJ and EYA developed and performed the 3D co-culture model. HY provided resources. All authors have read and agreed to the final version of the manuscript.

References

1. Siegel RL, Miller KD, Fuchs HE, Jemal A. Cancer statistics, 2022. CA Cancer J Clin 72, 7-33 (2022).

2. Bubendorf L, et al. Metastatic patterns of prostate cancer: an autopsy study of 1,589 patients. Hum Pathol 31, 578-583 (2000).

3. Berruti A, et al. Incidence of skeletal complications in patients with bone metastatic prostate cancer and hormone refractory disease: predictive role of bone resorption and formation markers evaluated at baseline. J Urol 164, 1248-1253 (2000).

4. Sartor O, de Bono JS. Metastatic Prostate Cancer. N Engl J Med 378, 645-657 (2018).

5. Uhr JW, Pantel K. Controversies in clinical cancer dormancy. Proc Natl Acad Sci U S A 108, 12396-12400 (2011).

6. Ruppender NS, Morrissey C, Lange PH, Vessella RL. Dormancy in solid tumors: implications for prostate cancer. Cancer Metastasis Rev 32, 501-509 (2013).

7. Aguirre-Ghiso JA. Models, mechanisms and clinical evidence for cancer dormancy. Nat Rev Cancer 7, 834-846 (2007).

8. Phan TG, Croucher PI. The dormant cancer cell life cycle. Nat Rev Cancer 20, 398-411 (2020).

9. Pfitzenmaier J, et al. Telomerase activity in disseminated prostate cancer cells. BJU Int 97, 1309-1313 (2006).

10. Thomas C, et al. Urokinase-plasminogen-activator receptor expression in disseminated tumour cells in the bone marrow and peripheral blood of patients with clinically localized prostate cancer. BJU Int 104, 29-34 (2009).

11. Weckermann D, Muller P, Wawroschek F, Harzmann R, Riethmuller G, Schlimok G. Disseminated cytokeratin positive tumor cells in the bone marrow of patients with prostate cancer: detection and prognostic value. J Urol 166, 699-703 (2001).

12. Murray NP. Minimal residual disease in prostate cancer patients after primary treatment: theoretical considerations, evidence and possible use in clinical management. Biol Res 51, 32 (2018).

13. Murray NP, et al. Minimal Residual Disease Defines the Risk and Time to Biochemical Failure in Patients with Pt2 and Pt3a Prostate Cancer Treated With Radical Prostatectomy: An Observational Prospective Study. Urol J 17, 262-270 (2020).

14. Decker AM, et al. Adrenergic Blockade Promotes Maintenance of Dormancy in Prostate Cancer Through Upregulation of GAS6. Transl Oncol 13, 100781 (2020).

15. Aguirre-Ghiso JA. How dormant cancer persists and reawakens. Science 361, 1314-1315 (2018).

16. Vera-Ramirez L. Cell-intrinsic survival signals. The role of autophagy in metastatic dissemination and tumor cell dormancy. Semin Cancer Biol 60, 28-40 (2020).

17. Datta SR, et al. Akt phosphorylation of BAD couples survival signals to the cell-intrinsic death machinery. Cell 91, 231-241 (1997).

18. Singh DK, Patel VG, Oh WK, Aguirre-Ghiso JA. Prostate Cancer Dormancy and Reactivation in Bone Marrow. J Clin Med 10, (2021).

19. Sosa MS, Bragado P, Aguirre-Ghiso JA. Mechanisms of disseminated cancer cell dormancy: an awakening field. Nat Rev Cancer 14, 611-622 (2014).

20. Albrengues J, et al. Neutrophil extracellular traps produced during inflammation awaken dormant cancer cells in mice. Science 361, (2018).

21. Giancotti FG. Mechanisms governing metastatic dormancy and reactivation. Cell 155, 750-764 (2013).

22. Lam HM, Vessella RL, Morrissey C. The role of the microenvironment-dormant prostate disseminated tumor cells in the bone marrow. Drug Discov Today Technol 11, 41-47 (2014).

23. Owen KL, et al. Prostate cancer cell-intrinsic interferon signaling regulates dormancy and metastatic outgrowth in bone. EMBO Rep 21, e50162 (2020).

24. Lee E, et al. Growth Arrest-Specific 6 (GAS6) Promotes Prostate Cancer Survival by G1 Arrest/S Phase Delay and Inhibition of Apoptosis During Chemotherapy in Bone Marrow. J Cell Biochem 117, 2815-2824 (2016).

25. Cackowski FC, et al. Mer Tyrosine Kinase Regulates Disseminated Prostate Cancer Cellular Dormancy. J Cell Biochem 118, 891-902 (2017).

26. Yumoto K, et al. Axl is required for TGF-beta2-induced dormancy of prostate cancer cells in the bone marrow. Sci Rep 6, 36520 (2016).

27. Murray NP, et al. Redefining micrometastasis in prostate cancer - a comparison of circulating prostate cells, bone marrow disseminated tumor cells and micrometastasis: Implications in determining local or systemic treatment for biochemical failure after radical prostatectomy. Int J Mol Med 30, 896-904 (2012).

28. Sharma S, et al. Regucalcin promotes dormancy of prostate cancer. Oncogene 40, 1012-1026 (2021).

29. Abida W, et al. Genomic correlates of clinical outcome in advanced prostate cancer. Proc Natl Acad Sci U S A 116, 11428-11436 (2019).

30. Sosa MS, et al. NR2F1 controls tumour cell dormancy via SOX9- and RARbeta-driven quiescence programmes. Nat Commun 6, 6170 (2015).

31. Bagi CM, Roberts GW, Andresen CJ. Dual focal adhesion kinase/Pyk2 inhibitor has positive effects on bone tumors: implications for bone metastases. Cancer 112, 2313-2321 (2008).

32. Roberts WG, et al. Antitumor activity and pharmacology of a selective focal adhesion kinase inhibitor, PF-562,271. Cancer Res 68, 1935-1944 (2008).

33. Sun H, Pisle S, Gardner ER, Figg WD. Bioluminescent imaging study: FAK inhibitor, PF-562,271, preclinical study in PC3M-luc-C6 local implant and metastasis xenograft models. Cancer Biol Ther 10, 38-43 (2010).

34. Grant GD, Kedziora KM, Limas JC, Cook JG, Purvis JE. Accurate delineation of cell cycle phase transitions in living cells with PIP-FUCCI. Cell Cycle 17, 2496-2516 (2018).

35. Tzaphlidou M. Bone architecture: collagen structure and calcium/phosphorus maps. J Biol Phys 34, 39-49 (2008).

36. Paschalis EP, Recker R, DiCarlo E, Doty SB, Atti E, Boskey AL. Distribution of collagen cross-links in normal human trabecular bone. J Bone Miner Res 18, 1942-1946 (2003).

37. Conway T, et al. Xenome--a tool for classifying reads from xenograft samples. Bioinformatics 28, i172-178 (2012).

38. Kluin RJC, et al. XenofilteR: computational deconvolution of mouse and human reads in tumor xenograft sequence data. BMC Bioinformatics 19, 366 (2018).

39. Bray NL, Pimentel H, Melsted P, Pachter L. Near-optimal probabilistic RNA-seq quantification. Nat Biotechnol 34, 525-527 (2016).

40. Venegas V, Halberg MC. Measurement of mitochondrial DNA copy number. Methods Mol Biol 837, 327-335 (2012).

41. Miyamoto DT, et al. RNA-Seq of single prostate CTCs implicates noncanonical Wnt signaling in antiandrogen resistance. Science 349, 1351-1356 (2015).

42. Huang S, Liu Y, Chen Z, Wang M, Jiang VC. PIK-75 overcomes venetoclax resistance via blocking PI3K-AKT signaling and MCL-1 expression in mantle cell lymphoma. Am J Cancer Res 12, 1102-1115 (2022).

43. Boire A, Coffelt SB, Quezada SA, Vander Heiden MG, Weeraratna AT. Tumour Dormancy and Reawakening: Opportunities and Challenges. Trends Cancer 5, 762-765 (2019).

44. Risson E, Nobre AR, Maguer-Satta V, Aguirre-Ghiso JA. The current paradigm and challenges ahead for the dormancy of disseminated tumor cells. Nat Cancer 1, 672-680 (2020).

45. Kollermann J, Heseding B, Helpap B, Kollermann MW, Pantel K. Comparative immunocytochemical assessment of isolated carcinoma cells in lymph nodes and bone marrow of patients with clinically localized prostate cancer. Int J Cancer 84, 145-149 (1999).

46. Manna F, et al. Metastases in Prostate Cancer. Cold Spring Harb Perspect Med 9, (2019).

47. Yu-Lee LY, et al. Osteoblast-Secreted Factors Mediate Dormancy of Metastatic Prostate Cancer in the Bone via Activation of the TGFbetaRIII-p38MAPK-pS249/T252RB Pathway. Cancer Res 78, 2911-2924 (2018).

48. Shiozawa Y, et al. Human prostate cancer metastases target the hematopoietic stem cell niche to establish footholds in mouse bone marrow. J Clin Invest 121, 1298-1312 (2011).

49. Ivey NS, et al. Association of FAK activation with lentivirus-induced disruption of blood-brain barrier tight junction-associated ZO-1 protein organization. J Neurovirol 15, 312-323 (2009).

50. Khoo WH, et al. A niche-dependent myeloid transcriptome signature defines dormant myeloma cells. Blood 134, 30-43 (2019).

51. Ren Q, Khoo WH, Corr AP, Phan TG, Croucher PI, Stewart SA. Gene expression predicts dormant metastatic breast cancer cell phenotype. Breast Cancer Res 24, 10 (2022).

52. Quayle LA, Spicer A, Ottewell PD, Holen I. Transcriptomic Profiling Reveals Novel Candidate Genes and Signalling Programs in Breast Cancer Quiescence and Dormancy. Cancers (Basel) 13, (2021).

53. Chery L, et al. Characterization of single disseminated prostate cancer cells reveals tumor cell heterogeneity and identifies dormancy associated pathways. Oncotarget 5, 9939-9951 (2014).

54. Borgen E, et al. NR2F1 stratifies dormant disseminated tumor cells in breast cancer patients. Breast Cancer Res 20, 120 (2018).

55. Gao XL, et al. NR2F1 contributes to cancer cell dormancy, invasion and metastasis of salivary adenoid cystic carcinoma by activating CXCL12/CXCR4 pathway. BMC Cancer 19, 743 (2019).

56. Rodriguez-Tirado C, et al. NR2F1 Is a Barrier to Dissemination of Early-Stage Breast Cancer Cells. Cancer Res 82, 2313-2326 (2022).

57. Khalil BD, et al. An NR2F1-specific agonist suppresses metastasis by inducing cancer cell dormancy. J Exp Med 219, (2022).

58. Jakob M, et al. Role of cancer stem cell markers ALDH1, BCL11B, BMI-1, and CD44 in the prognosis of advanced HNSCC. Strahlenther Onkol 197, 231-245 (2021).

59. Federer-Gsponer JR, et al. Patterns of stemness-associated markers in the development of castration-resistant prostate cancer. Prostate 80, 1108-1117 (2020).

60. Xue C, Corey E, Gujral TS. Proteomic and Transcriptomic Profiling Reveals Mitochondrial Oxidative Phosphorylation as Therapeutic Vulnerability in Androgen Receptor Pathway Active Prostate Tumors. Cancers (Basel) 14, (2022).

61. Becker M, Nitsche A, Neumann C, Aumann J, Junghahn I, Fichtner I. Sensitive PCR method for the detection and real-time quantification of human cells in xenotransplantation systems. Br J Cancer 87, 1328-1335 (2002).

62. Subramanian G, Elsaadany M, Bialorucki C, Yildirim-Ayan E. Creating homogenous strain distribution within 3D cell-encapsulated constructs using a simple and cost-effective uniaxial tensile bioreactor: Design and validation study. Biotechnol Bioeng 114, 1878-1887 (2017).

63. Elsaadany M, Harris M, Yildirim-Ayan E. Design and Validation of Equiaxial Mechanical Strain Platform, EQUicycler, for 3D Tissue Engineered Constructs. Biomed Res Int 2017, 3609703 (2017).

64. Elsaadany M, Yan KC, Yildirim-Ayan E. Predicting cell viability within tissue scaffolds under equiaxial strain: multi-scale finite element model of collagen-cardiomyocytes constructs. Biomech Model Mechanobiol 16, 1049-1063 (2017).

65. Baylan N, Bhat S, Ditto M, Lawrence JG, Lecka-Czernik B, Yildirim-Ayan E. Polycaprolactone nanofiber interspersed collagen type-I scaffold for bone regeneration: a unique injectable osteogenic scaffold. Biomed Mater 8, 045011 (2013).

66. Al-Mamun MA, et al. Characterization and evaluation of antibacterial and antiproliferative activities of crude protein extracts isolated from the seed of Ricinus communis in Bangladesh. BMC Complement Altern Med 16, 211 (2016).

67. Kim D, Paggi JM, Park C, Bennett C, Salzberg SL. Graph-based genome alignment and genotyping with HISAT2 and HISAT-genotype. Nat Biotechnol 37, 907-915 (2019).

68. Liao Y, Smyth GK, Shi W. featureCounts: an efficient general purpose program for assigning sequence reads to genomic features. Bioinformatics 30, 923-930 (2014).

69. Shen W, Le S, Li Y, Hu F. SeqKit: A Cross-Platform and Ultrafast Toolkit for FASTA/Q File Manipulation. PLoS One 11, e0163962 (2016).

70. Chen EY, et al. Enrichr: interactive and collaborative HTML5 gene list enrichment analysis tool. BMC Bioinformatics 14, 128 (2013).

71. Ge SX, Jung D, Yao R. ShinyGO: a graphical gene-set enrichment tool for animals and plants. Bioinformatics 36, 2628-2629 (2020).

72. Su S, et al. Enzalutamide-induced and PTH1R-mediated TGFBR2 degradation in osteoblasts confers resistance in prostate cancer bone metastases. Cancer Lett 525, 170-178 (2022).

Figures

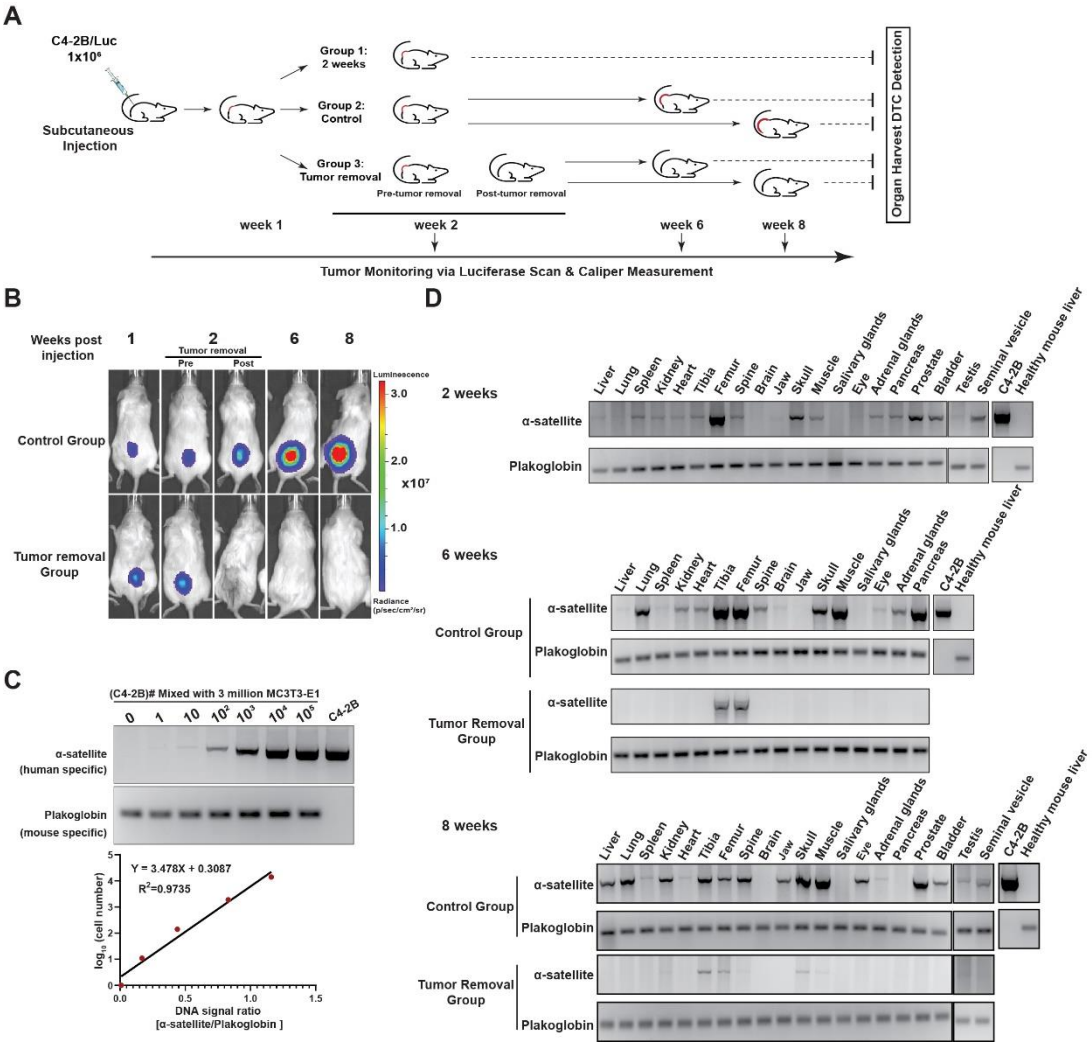

Figure 1. Disseminated PCa cells were limited in bones after primary tumor removal

A. The experimental design. **B**. Representative weekly luminescent imaging of subcutaneous tumor grown in mice. **C**. Species-specific PCR for standard. **D**. Species-specific PCR. 2 μg total genomic DNA for α-satellite PCR and 0.5 μg total genomic DNA for plakoglobin PCR were optimized. n=4 for groups at 2/6 weeks and n=3 for groups at 8 weeks. PCR were performed with triplicates.

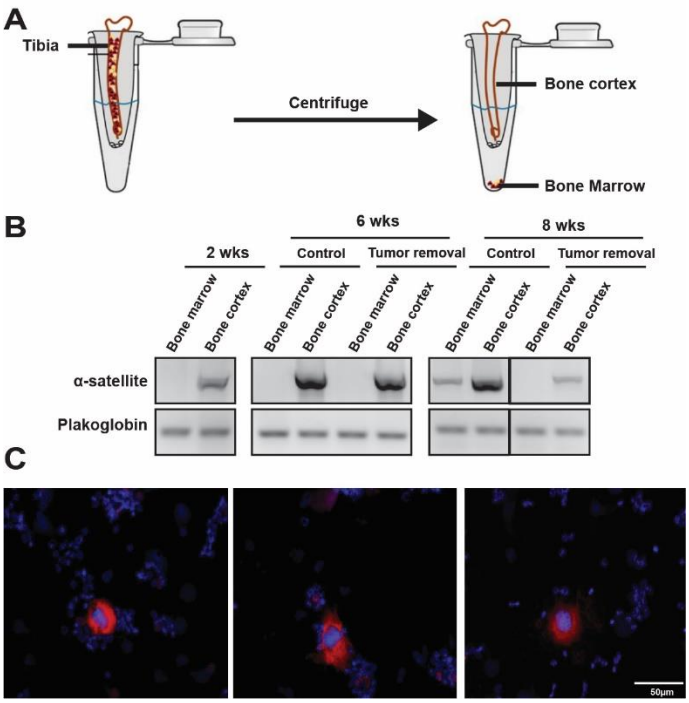

Figure 2. Disseminated PCa cells were detected in bone cortex versus in bone marrow

A. Diagram of separation for the bone cortex and bone marrow of mouse long bones. **B.** Species-specific PCR. **C.** IF staining of bone marrow using human species-specific mitochondrial antibody. n≥3 and PCR were performed with triplicates.

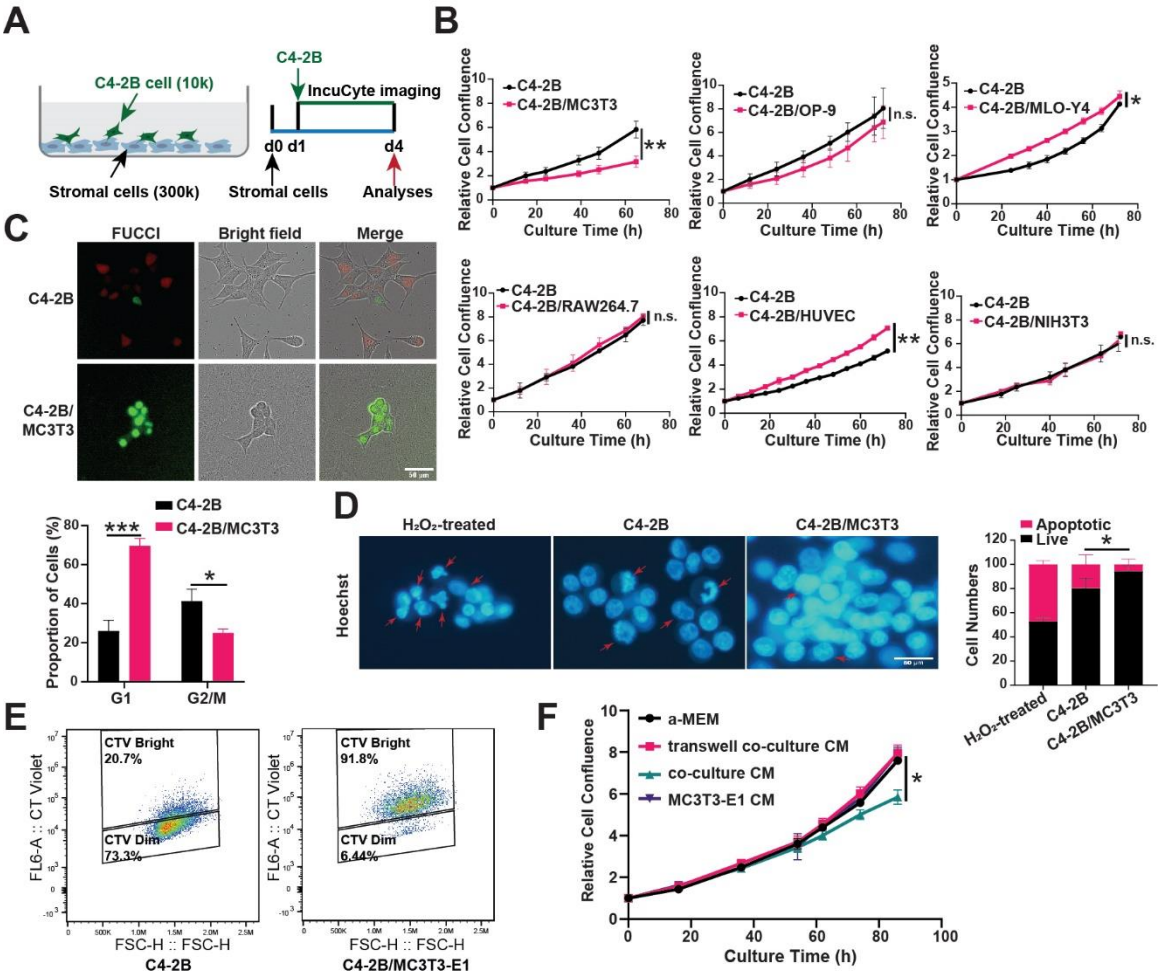

Figure 3. MC3T3-E1 decreased the cell proliferation and apoptosis of C4-2B cells in the mixed co-culture

A. The experimental design for the mixed co-culture. **B**. MC3T3-E1 cells, but not other types of cells, inhibited the cell proliferation. **C**. G1 cell cycle arrest. Representative fluorescent and bright field pictures were shown. Pure green are cells in G1 phase and pure red are cells in M phase. **D**. Cell apoptosis. Representative pictures were shown. DAPI was used to stain the cell nucleus, arrows indicated the apoptotic cells based on the nuclear phenotype. **E**. Cell division. C4-2B cells were saturated with CellTrace™ Violet membrane dye and the signal intensity in each cell was captured using Flow cytometry. **F**. Conditioned media (CM) only from the mixed co-culture inhibited cell proliferation. n≥3 with triplicates. * $p < 0.05$, ** $p < 0.01$, *** $p < 0.001$.

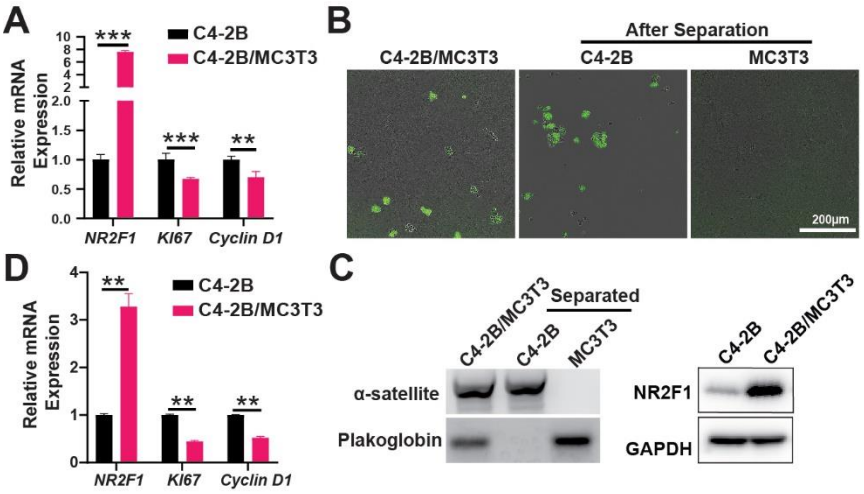

Figure 4. Increased expression of dormancy marker and decreased expression of proliferation markers of C4-2B cells in the mixed co-culture with MC3T3-E1 cells

A. MC3T3-E1 cells increased NR2F1 but decreased Ki67 and cyclin D1 transcripts. Species-specific qRT-PCRs and relative fold changes of the genes were performed and analyzed. **B**. Representative pictures after separation of C4-2B cells (GFP labeled) from MC3T3-E1 cells (not labeled). **C**. Left panel, species-specific PCR was used to further confirm the separation of cells. Right panel, MC3T3-E1 cells increased NR2F1 at protein level. **D**. MC3T3-E1 cells increased NR2F1 but decreased Ki67 and cyclin D1 transcripts in 3D co-culture model. Species-specific qRT-PCRs and relative fold changes of the genes were performed and analyzed. n≥3 with triplicates, ** $p < 0.01$, *** $p < 0.001$.

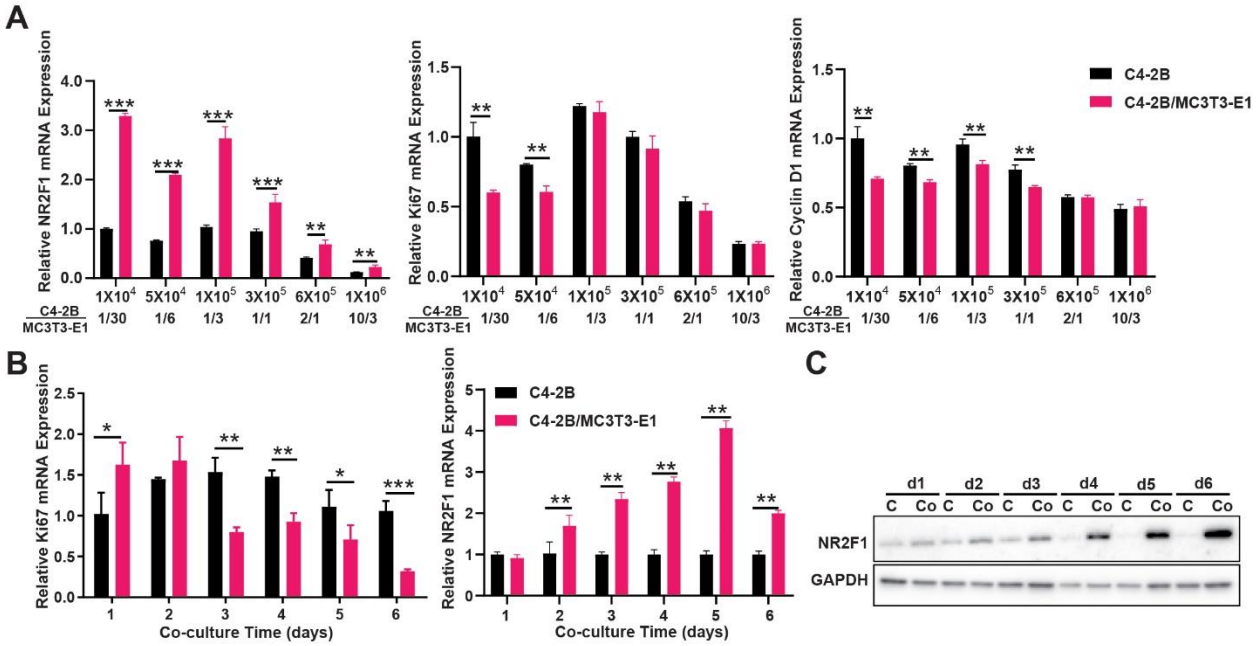

Figure 5. Range of cell numbers and times for the mixed co-culture of C4-2B and MC3T3-E1 cells

Gene expression of dormancy and proliferation markers were explored under various cell numbers **A** and culture times **B** in the mixed co-cultures using species-specific qRT-PCRs. **C**. Time-dependent NR2F1 protein in C4-2B cells from the mixed co-culture. n≥3 with triplicates, * $p < 0.05$, ** $p < 0.01$, *** $p < 0.001$.

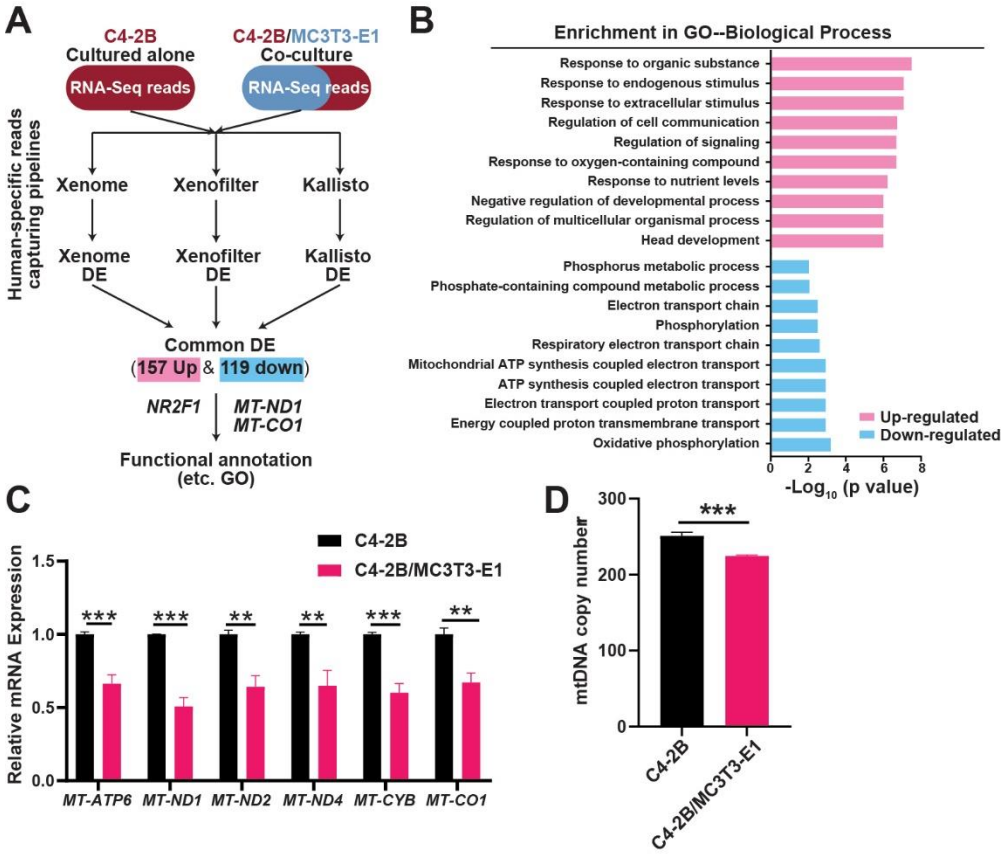

Figure 6. Mitochondrial genes were decreased in dormant C4-2B cells

A. Workflow of RNA-sequencing date analyses. **B**. GO classification of biological process in dormant C4-2B cells via ShinyGO v0.61. **C**. Mitochondrial genes involved in the enriched biological process were decreased in the co-cultured C4-2B cells, in relative to the cultured alone. Species-specific qRT-PCRs and relative fold changes of the genes were performed and analyzed. **D**. mtDNA copy numbers were decreased in the co-cultured C4-2B cells, in relative to the cultured alone. $n \geq 3$ with triplicates, ** $p < 0.01$, *** $p < 0.001$.

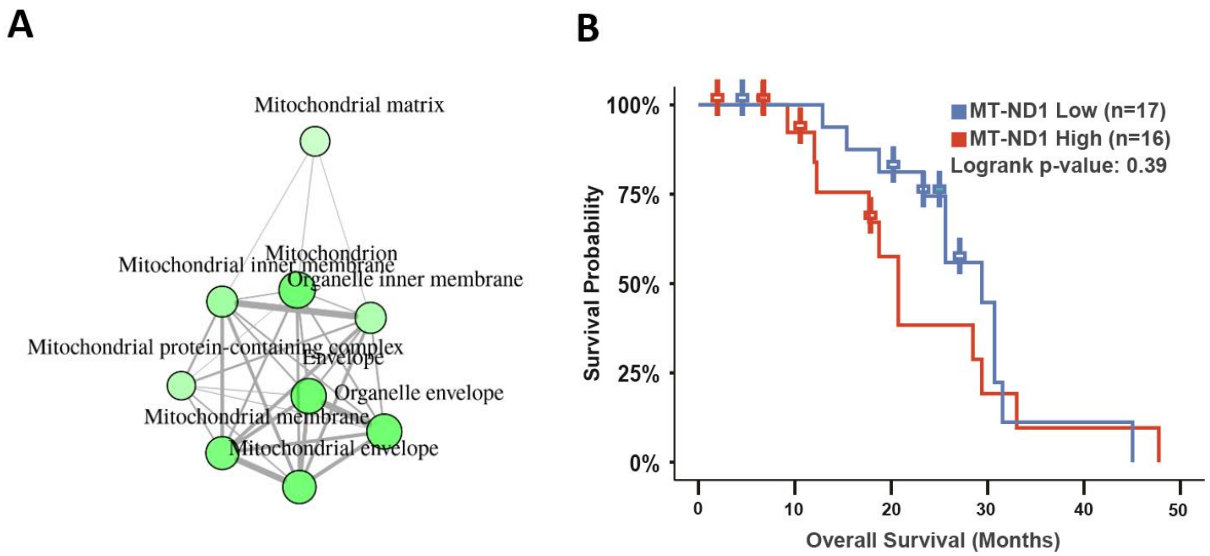

Figure 7. Mitochondrial genes were correlated to PCa progression from clinical datasets.

A. Upregulated DE genes in circulating tumor cells were enriched to the mitochondrial structural components (data processed from previously published study [41], plot generated with ShinyGO v0.61). **B.** Patients with *MT-ND1* gene expression at low level, compared to patients expressed *MT-ND1* at high level, has a favorable prognostic trend in PCa patients with bone metastases n=16 high vs n= 17 low, P= 0.39, from cBioportal study ID: prad_su2c_2019.

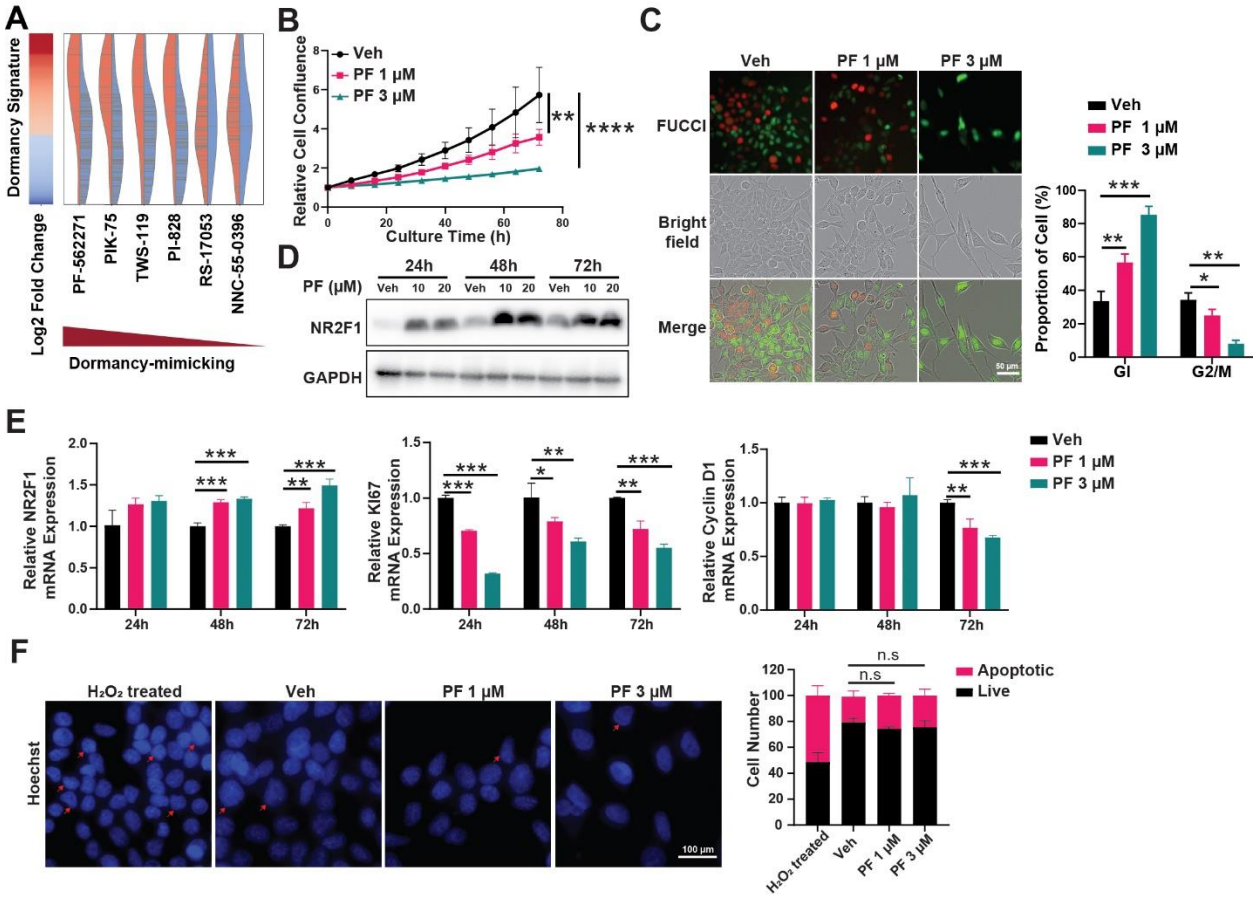

Figure 8. PF-562271 inhibited the cell proliferation and enriched C4-2B cells in G1 phase.

A. Top list of AI predicted potential dormancy-mimicking drugs based on the dormant gene signature of C4-2B cells in the mixed co-culture. **B**. Effects of PF-567721 on cell proliferation. **C**. Representative fluorescent and bright field pictures. **D**. Effects of PF-567721 on the expression of NR2F1 in protein level. **E**. Effects of PF-567721 on NR2F1, KI67, and Cyclin D1 mRNA expression. **F**. Representative pictures of PF-567721 effects on apoptosis. Hoechst was used to stain the cell nuclei; red arrows pointed the apoptotic cells. n≥3 with triplicates, * $p < 0.05$, ** $p < 0.01$, *** $p < 0.001$, **** $p < 0.0001$, and n.s. non-significant.

Supplementary Figures

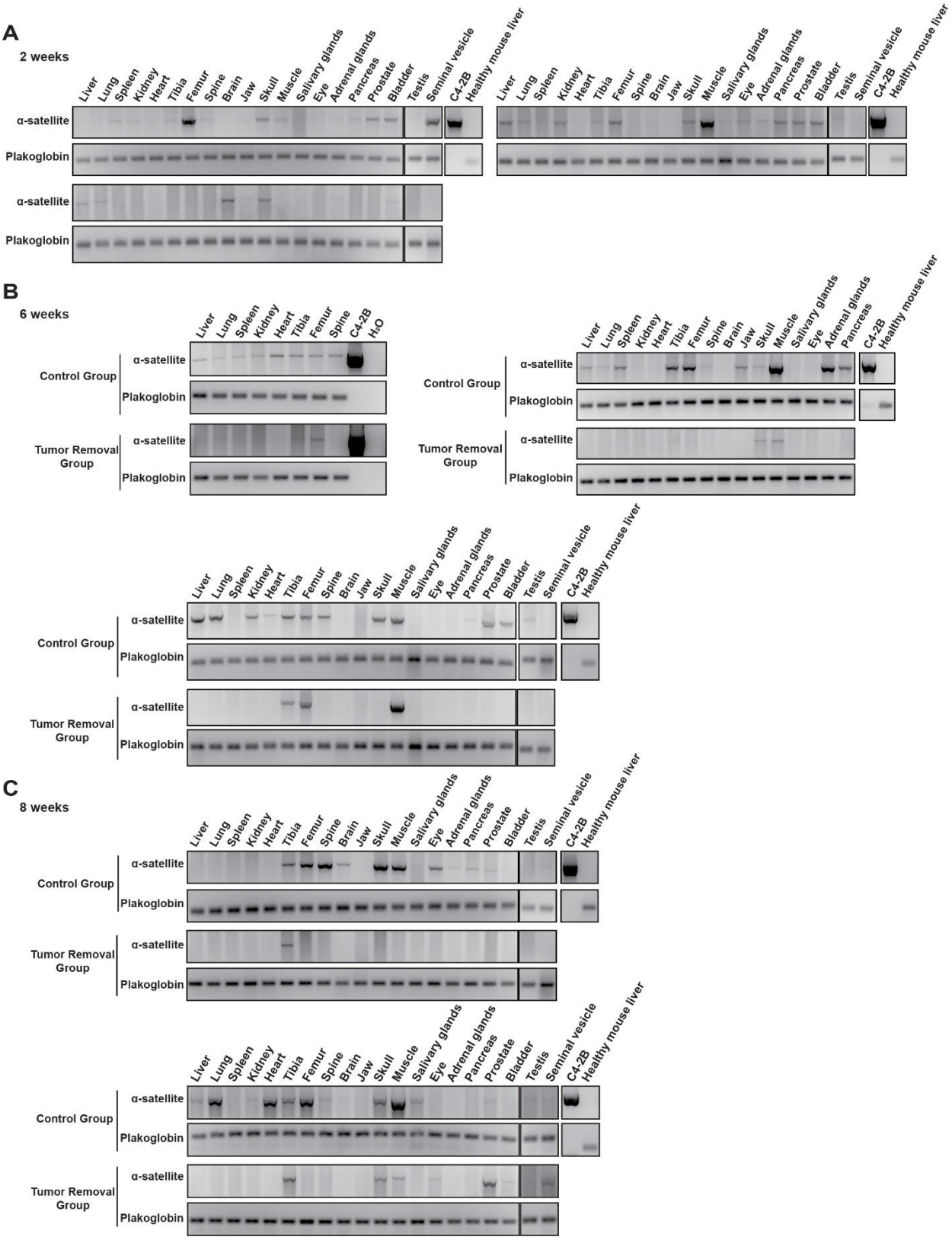

Supplementary Figure S1. Gel pictures of DTC detection using species-specific PCR from each mouse

2 wks post injection (**A**), 6 wks post injection (**B**), and 8 wks (**C**) post injection.

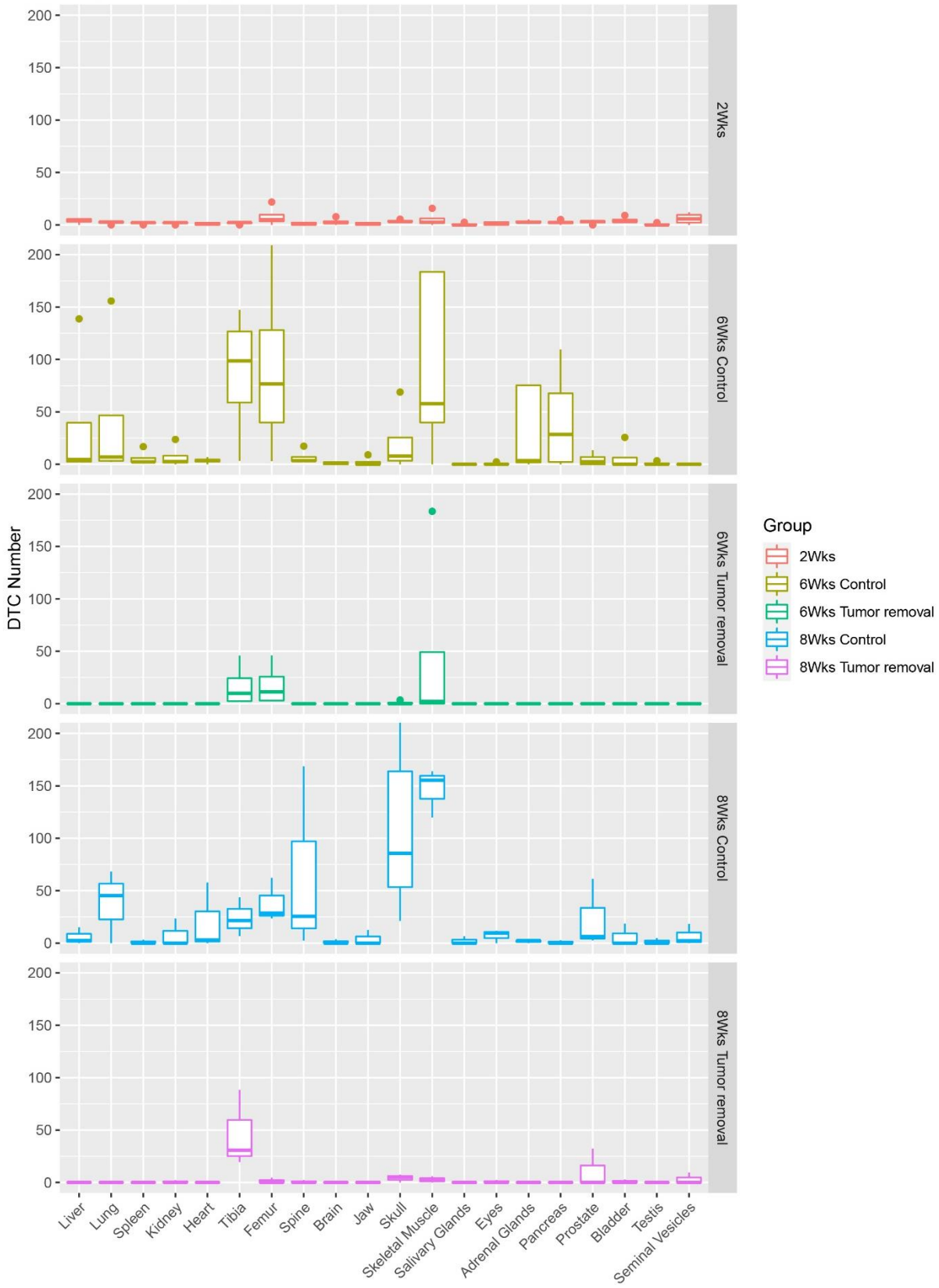
DTC Number
200
150
100
50
0
2Wks
6Wks Control
6Wks Tumor removal
8Wks Control
8Wks Tumor removal
Liver
Lung
Spleen
Kidney
Heart
Tibia
Femur
Spine
Brain
Jaw
Skull
Skeletal Muscle
Salivary Glands
Eyes
Adrenal Glands
Pancreas
Prostate
Bladder
Testis
Seminal Vesicles
Group
2Wks
6Wks Control
6Wks Tumor removal
8Wks Control
8Wks Tumor removal

Supplementary Figure S2. Quantification of DTC in various organs post subcutaneous C4-2B tumor xenograft and removal.

DTC numbers were calculated using the PCR band intensities shown in **Figure 1D** and **Figure S1** based on the standards. The plot was created via ggplot2 in R.

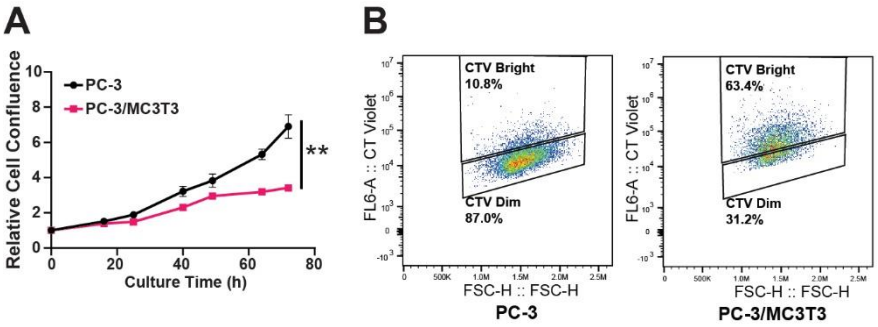

Supplementary Figure S3. MC3T3-E1 inhibited the cell proliferation of PC-3 cells in the mixed co-culture

A. Cell proliferation. **B**. Cell division. n≥3 with triplicates, ** $p < 0.01$.

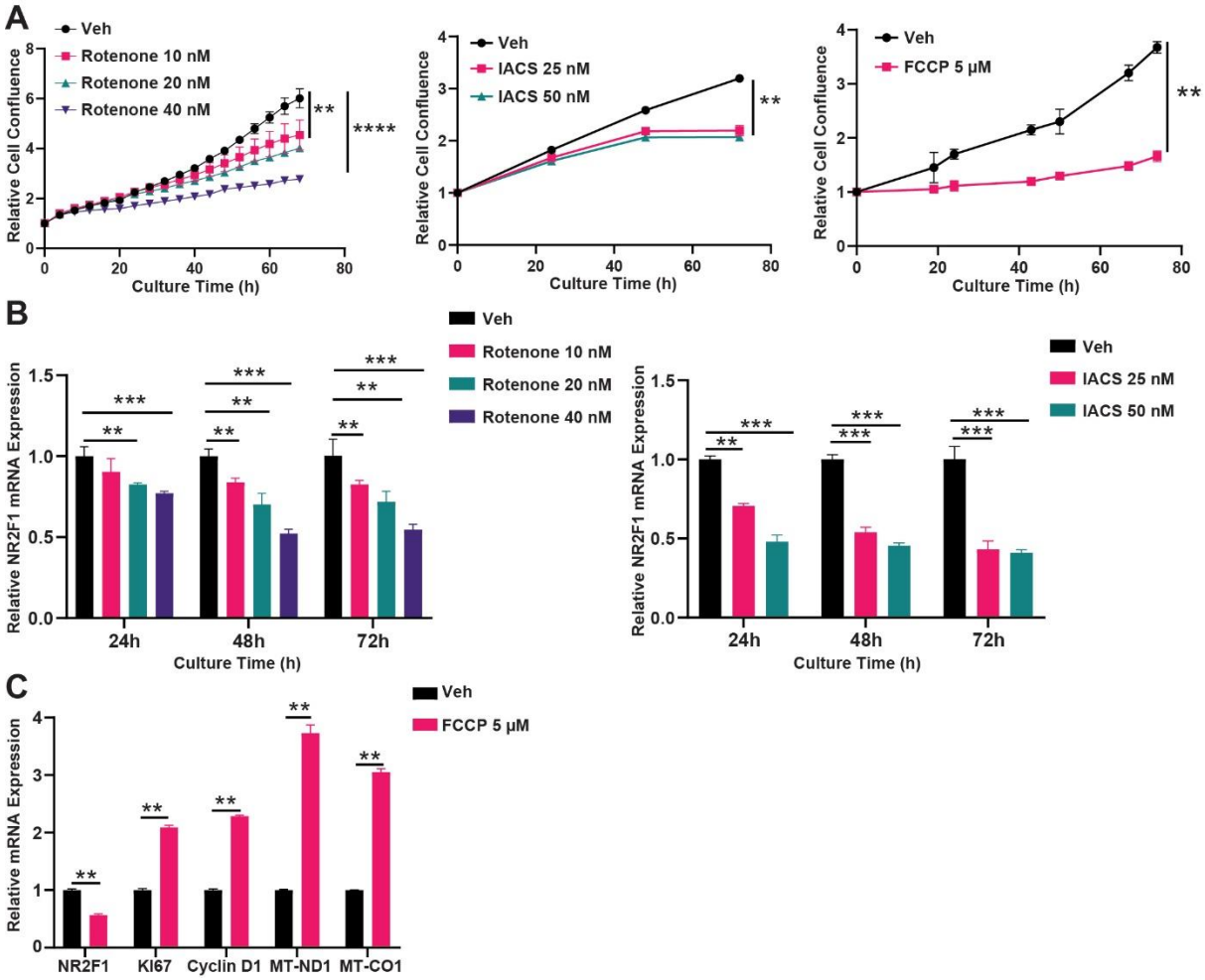

Supplementary Figure S4. Mitochondrial inhibitors inhibited C4-2B cell proliferation but not induced dormancy

A. Effects of mitochondrial inhibitors, Rotenone, IACS, and FCCP, on cell proliferation. **B**. Time- and dose-dependent effects of Rotenone (Left panel) or IACS (Right panel) on NR2F1 at mRNA level. **C**. Effects of FCCP on gene expressions at 72 hours. n≥3 with triplicates, * $p < 0.05$, ** $p < 0.01$, *** $p < 0.001$, **** $p < 0.0001$.

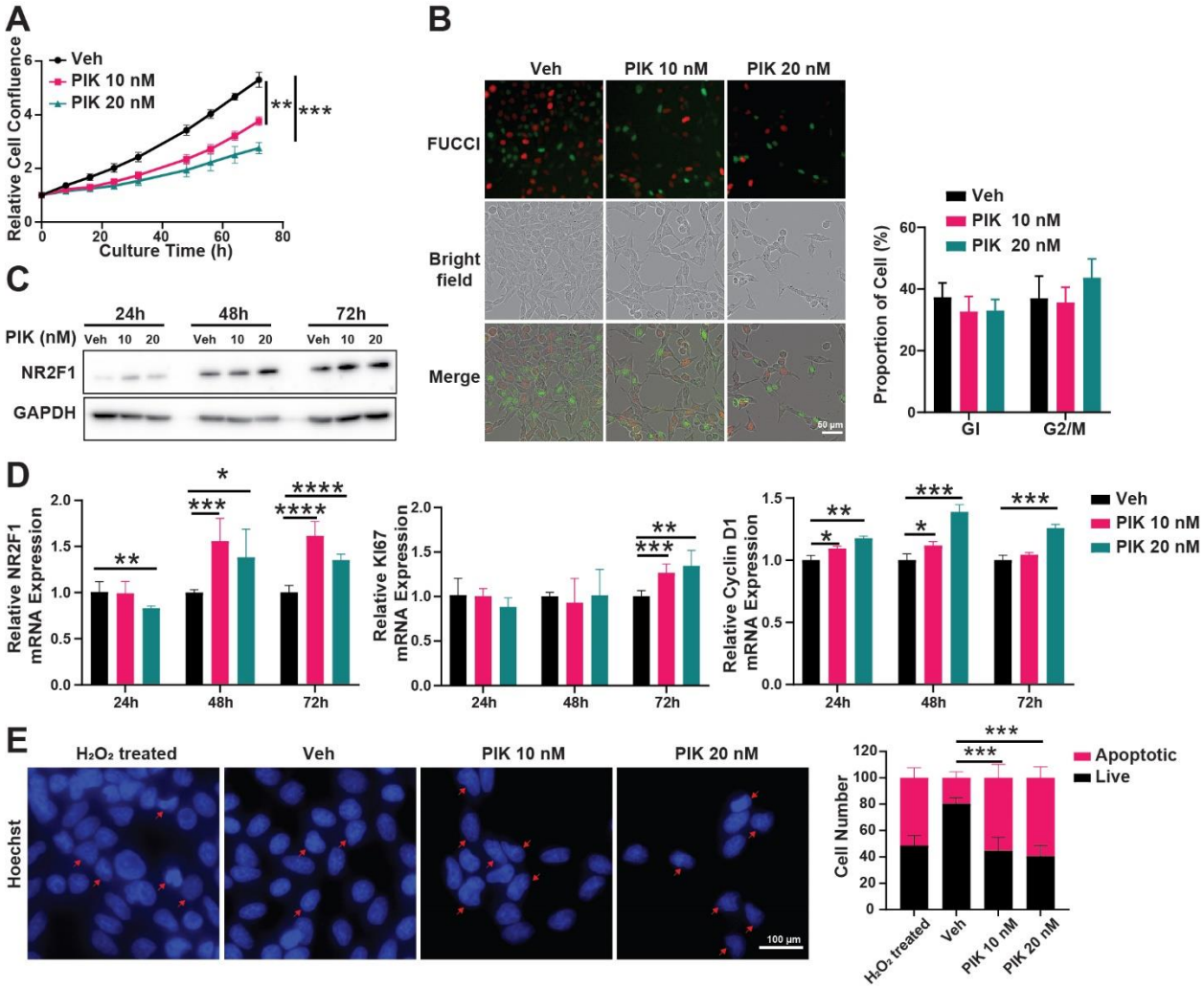

Supplementary Figure S5. PIK-75 inhibited C4-2B cells proliferation but not induced dormancy

A.PIK-75 inhibited the cell proliferation. **B**. PIK-75 did not cause cell cycle arrest. Representative fluorescent and bright field pictures were shown. **C**. Effects of PIK-75 on the expression of NR2F1 at protein level. **D**. Time- and dose-dependent effect of PIK-75 on NR2F1, Ki67, and Cyclin D1 at mRNA level. **E**. Effect of PIK-75 on apoptosis. Representative pictures were shown. Hoechst was used to stain the cell nuclei; red arrows pointed the apoptotic cells. Average apoptotic C4-2B cell numbers in each group were ploted. n≥3 with triplicates, * $p < 0.05$, *** $p < 0.01$, *** $p < 0.001$.

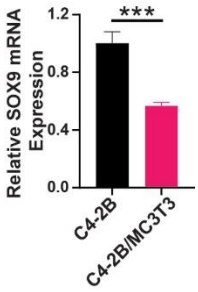

Supplementary Figure S6. SOX9 was decreased in C4-2B cells in the mixed co-culture with MC3T3-E1

Species-specific qRT-PCR were performed. n≥3 with triplicates, *** $p < 0.001$.